5188 *Biochemistry* **2010,** *49,* 5188–5199
DOI: 10.1021/bi100555q

BIOCHEMISTRY
including biophysical chemistry & molecular biology
Article

Valine 375 and Phenylalanine 109 Confer Affinity and Specificity for Pyruvate as Donor Substrate in Acetohydroxy Acid Synthase Isozyme II from *Escherichia coli*[†]

Andrea Steinmetz,[‡,⊥] Maria Vyazmensky,[§,⊥] Danilo Meyer,[‡] Ze′ev Barak,[§] Ralph Golbik,[∥] David M. Chipman,*[,§] and Kai Tittmann*[,‡]

[‡]*Albrecht-von-Haller-Institute and Göttingen Centre for Molecular Biosciences, Ernst-Caspari-Haus, Department of Bioanalytics, Georg-August University Göttingen, Justus-von-Liebig Weg 11, 37077 Göttingen, Germany,* [§]*Department of Life Sciences, Ben-Gurion University of the Negev, Beer-Sheva 84105, Israel, and* [∥]*Institute for Biochemistry and Biotechnology, Martin-Luther University Halle-Wittenberg, Kurt-Mothes-Strasse 3, 06120 Halle/Saale, Germany.* [⊥]*Both authors contributed equally to this work.*

Received April 12, 2010; Revised Manuscript Received May 26, 2010

ABSTRACT: Acetohydroxy acid synthase (AHAS) is a thiamin diphosphate-dependent enzyme that catalyzes the condensation of pyruvate with either another pyruvate molecule (product acetolactate) or 2-ketobutyrate (product acetohydroxybutyrate) as the first common step in the biosynthesis of branched-chain amino acids in plants, bacteria, algae, and fungi. AHAS isozyme II from *Escherichia coli* exhibits a 60-fold higher specificity for 2-ketobutyrate (2-KB) over pyruvate as acceptor, which was shown to result from a stronger hydrophobic interaction of the ethyl substituent of 2-KB with the side chain of Trp464 in multiple, apparently committed steps of catalysis. Here, we have elucidated the molecular determinants conferring specificity for pyruvate as the sole physiological donor substrate. Structural studies and sequence alignments of the POX subfamily of ThDP enzymes that act on pyruvate indicate that a valine and a phenylalanine hydrophobically interact with the methyl substituent of pyruvate. Kinetic and thermodynamic studies on AHAS isozyme II variants with substitutions at these positions (Val375Ala, Val375Ile, and Phe109Met) were carried out. While Val375 variants exhibit a slightly reduced k_{cat} with a moderate increase of the apparent K_M of pyruvate, both substrate affinity and k_{cat} are significantly compromised in AHAS Phe109Met. The specificity for 2-ketobutyrate as acceptor is not altered in the variants. Binding of acylphosphonates as analogues of donor substrates was analyzed by circular dichroism spectroscopy and stopped-flow kinetics. While binding of the pyruvate analogue is 10−100-fold compromised in all variants, Val375Ala binds the 2-KB analogue better than the wild type and with higher affinity than the pyruvate analogue, suggesting steric constraints imposed by Val375 as a major determinant for the thermodynamically favored binding of pyruvate in AHAS. NMR-based intermediate analysis at steady state reveals that a mutation of either Val375 or Phe109 is detrimental for unimolecular catalytic steps in which tetrahedral intermediates are involved, such as substrate addition to the cofactor and product liberation. This observation implies Val375 and Phe109 to not only conjointly mediate substrate binding and specificity but moreover to ensure a proper orientation of the donor substrate and intermediates for correct orbital alignment in multiple transition states.

Acetohydroxy acid synthase (AHAS,[1] EC 2.2.1.6) is a key enzyme for the biosynthesis of the branched-chain amino acids (BCAA) valine, leucine, and isoleucine as well as biosynthetic precursors derived from the same pathway (i.e., coenzyme A and pantothenate) in plants, bacteria, algae, and fungi (Figure 1) (*1*−*3*). AHAS requires thiamin diphosphate (ThDP), a divalent metal ion, and flavin adenine dinucleotide (FAD) as bioorganic cofactors although the flavin has no catalytic function and fulfills structural purposes (*4*, *5*). AHAS catalyzes the specific condensation of pyruvate (referred to as "donor" or "first substrate" in the following) with a second 2-keto acid ("acceptor" or "second substrate") which may be either another pyruvate molecule to give (*S*)-acetolactate or, alternatively, 2-ketobutyrate (2-KB) to yield (*S*)-acetohydroxybutyrate.

The catalytic cycle of AHAS (Figure 2) commences with binding of pyruvate to the active center (K_1) and subsequent carbonyl addition to the C2 carbanion of ThDP (k'_2) yielding the tetrahedral intermediate 2-lactyl-ThDP (LThDP). Decarboxylation of the latter (k'_3) gives the 2-hydroxyethyl-ThDP (HEThDP) enamine intermediate, which then undergoes carboligation with either pyruvate or 2-KB (k'_4) as alternative acceptors. Eventual liberation of the product from the resultant covalent acetohydroxy acid-ThDP (AHA-ThDP) intermediate (k'_5) completes the catalytic cycle.

[†]This work was supported by Deutsche Forschungsgemeinschaft Grant Ti 324/3-1 (to K.T.).

*To whom correspondence shall be addressed. K.T.: e-mail, ktittma@gwdg.de; phone, ++49-551-39 14430; fax, ++49-551-39 5749. D.M.C.: e-mail, chipman@bgu.ac.il; phone, ++ 972-8-647 2646; fax, ++ 972-8-646 1710.

[1]Abbreviations: AHAS, acetohydroxy acid synthase; BCAA, branched-chain amino acids; AHA, acetohydroxy acid; AL, acetolactate; AHB, acetohydroxybutyrate; PHB, propionohydroxybutyrate; 2-KB, 2-ketobutyrate; MAP, methyl acetylphosphonate; MPP, methyl propionylphosphonate; ThDP, thiamin diphosphate; LThDP, 2-lactyl-ThDP; HEThDP, 2-hydroxyethyl-ThDP; AHAThDP, covalent product−ThDP adduct between acetohydroxy acids and ThDP; ALThDP, covalent adduct between ThDP and product AL; AHBThDP, covalent adduct between ThDP and product AHB; FAD, flavin adenine dinucleotide; GCL, glyoxylate carboligase; POX, pyruvate oxidase; PDC, pyruvate decarboxylase; TK, transketolase.

 Published on Web 05/26/2010

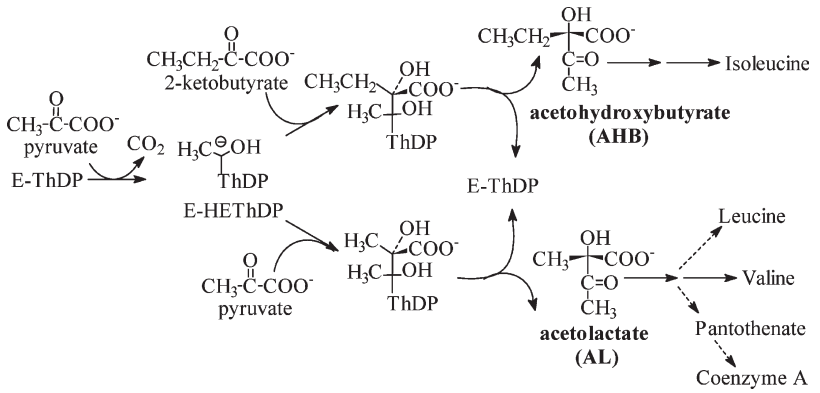

FIGURE 1: The alternative physiological reactions catalyzed by AHAS and the metabolic roles of the resultant products.

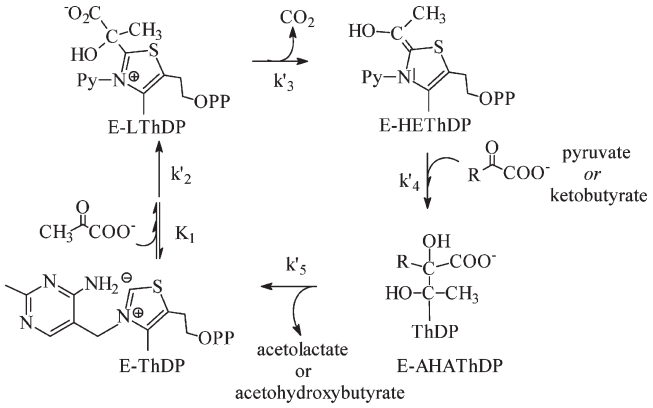

FIGURE 2: Minimal catalytic cycle of AHAS with intermediates and net rate constants identified. The covalent product−ThDP adduct AHAThDP will be either ALThDP (pyruvate as acceptor) or AHBThDP (2-KB as acceptor), respectively.

While pyruvate is the sole physiological donor substrate, many AHASs exhibit a higher preference for 2-KB as an acceptor, which ensures a balanced formation of both alternative products (and therewith all BCAAs) despite markedly lower intracellular concentrations of 2-KB compared to pyruvate (*6*). In the case of *Escherichia coli*, two of the three isozymes in total (AHASs II and III) prefer 2-KB 50−60-fold over pyruvate as an acceptor, whereas no such preference is observed for isozyme I (*1*, *7*). Mechanistic studies on AHAS II from *E. coli* identified tryptophan 464 to be a key player that mediates preferential binding of 2-KB because the hydrophobic interaction of its indole ring with the substrate substituent (ethyl in the case of 2-KB and methyl in the case of pyruvate) is more favorable for 2-KB (*8*). Substitution of Trp464 by leucine abrogated specificity of AHAS II for 2-KB (*9*). NMR-based analysis of reaction intermediates revealed that carboligation (condensation of the acceptor with the thiamin-bound first substrate) and product liberation are committed with Trp464 being involved in all of these steps, tempting us to propose a kinetic proofreading mechanism (*8*).

While AHASs prefer to bind and convert pyruvate and 2-KB as alternative acceptor substrates, with the latter being heavily favored in most cases, the enzymes must ensure a high preference for pyruvate as the first substrate to avoid nonphysiological condensation of two 2-KB molecules (product propionohydroxybutyrate, PHB) or of 2-KB as donor and pyruvate as acceptor (product propionolactate). Paraphrased, the active center of AHASs must have evolved such that pyruvate is heavily favored over 2-KB as donor, whereas the opposite preference must be generated for the acceptor. This constitutes a severe challenge with which AHASs have to deal because both potential substrates differ by just one methyl group and the individual binding pockets for donor and acceptor are located in close proximity.

To date, there is no high-resolution structure available for the catalytic subunit (CSU) of any of the three *E. coli* AHAS isozymes, but the X-ray structures of several homologous CSUs (yeast, *Arabidopsis thaliana*) were determined in complex with inhibitors, providing insights into the spatial architecture of the active site (*10*−*12*). In addition, X-ray crystallographic snapshots of reaction intermediates in the related enzyme pyruvate oxidase (POX) delineated the stereochemical course in pyruvate-processing ThDP enzymes and identified interactions between the intermediates and the protein (*13*, *14*). As shown in Figure 3, the substrate methyl substituent of LThDP in POX is accommodated in a hydrophobic pocket formed by Val394, Phe121, and the dimethylbenzene part of the flavin's isoalloxazine ring. A superposition of the active site of POX with that of yeast CSU AHAS suggests a similar substrate binding mode and interactions in both proteins. A sequence alignment of different ThDP enzymes including AHASs and POXs demonstrates that both the Val and Phe residues belonging to the hydrophobic patch (substrate substituent subsite) are highly conserved. It is significant that in the related enzyme glyoxylate carboligase (GCL), which contains the same cofactor set but acts on glyoxylate with a proton as substrate substituent rather than a methyl group, an isoleucine residue replaces the otherwise conserved valine (*15*). This clearly hints to a central role of this residue for substrate specificity, whereas the conserved Phe appears to have a more general role for substrate binding.

Here, we have examined AHAS isozyme II variants with substitutions in the donor substrate substituent subsite (Val375 and Phe109) by means of steady-state kinetics and NMR intermediate analysis at steady state plus thermodynamic and transient kinetic studies on phosphonate-based substrate analogues suitable to single out the binding process of the donor substrate and to gather insights into the individual contributions for substrate binding and specificity. In this context, we have considered AHAS II variants in which the donor substrate CH_3 substituent pocket is either enlarged (Val375Ala) or reduced (Val375Ile). In view of the putative general role of Phe109 for substrate binding, we have replaced this residue by a methionine (Phe109Met) that roughly occupies the same volume but is less hydrophobic.

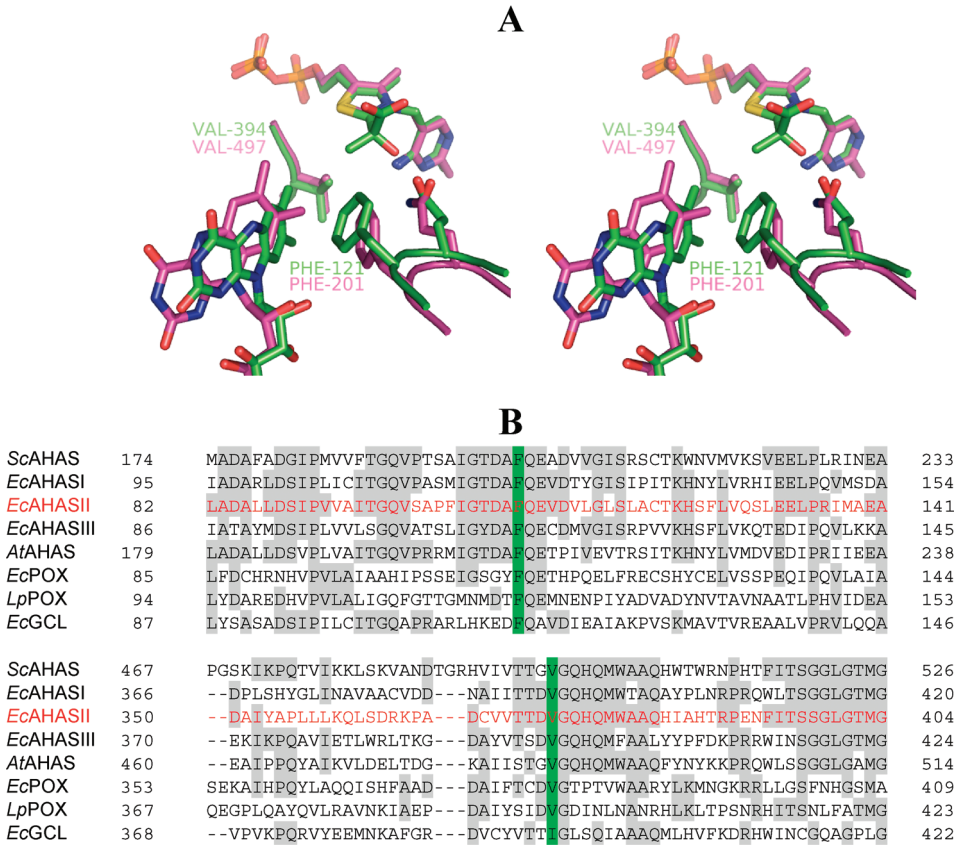

FIGURE 3: (A) Superposition of the active site of the yeast AHAS catalytic subunit (magenta) with that of *Lactobacillus plantarum* POX (green) with the trapped intermediate LThDP in stereoview. (B) Sequence alignment of different AHASs, POXs, and GCL as determined by the program ClustalW showing those regions that contain the conserved Val/Ile and Phe residues (both highlighted in green) of the donor binding site. The sequence of AHAS isozyme II from *E. coli* is indicated in red. Conserved residues are highlighted by a gray background.

MATERIALS AND METHODS

Chemicals and Reagents. Sodium 2-KB and ThDP were obtained from Sigma-Aldrich Chemie GmbH; IPTG, imidazole, and FAD were from AppliChem GmbH. Sodium pyruvate and magnesium sulfate heptahydrate were purchased from Merck; Ni−agarose superflow was supplied from Qiagen. Sulfometuron methyl (SMM) was a gift of Dr. J. V. Schloss, then of E. I. DuPont and Co., Central R&D Department, Wilmington, DE. All other chemicals and reagents were of analytical grade and were purchased from VWR International GmbH, Sigma-Aldrich Chemie GmbH, Carl Roth GmbH, and AppliChem GmbH. Quartz double-distilled water was used throughout the experiments.

Synthesis of Substrate Phosphonate Analogues. Methyl acetylphosphonate (MAP) and methyl propionylphosphonate (MPP) as analogues of pyruvate and 2-KB were synthesized using trimethyl phosphite and acetyl chloride (MAP) or propionyl chloride (MPP) as reagents according to ref *16*. Purity and correct synthesis of both compounds were confirmed by NMR spectroscopy and mass spectrometry.

Plasmids. Mutations were introduced into plasmid pQEV-GM encoding both the CSU and regulatory subunit (RSU) (*17*) at positions that correspond to residues Val375 and Phe109 using the QuikChange site-directed mutagenesis kit (Stratagene, La Jolla, CA). The correctness of the mutation was confirmed by complete sequencing of the plasmid.

Protein Expression and Purification. *E. coli* SG13009 cells carrying plasmid pQEV-GM were grown in LB medium (1% (w/v) tryptone, 0.5% (w/v) yeast extract, 0.5% (w/v) NaCl) and further containing ampicillin (100 μg/mL) and kanamycin (50 μg/mL) at 37 °C. Gene expression was induced at an OD_{600nm} of ~0.5 by addition of 0.4 mM IPTG, and cells were grown for 3 h at 37 °C. Cells were then harvested by centrifugation, shock-frozen in liquid nitrogen, and stored at −20 °C. For enzyme preparation, cells were thawed on ice and resuspended in buffer A (0.1 M potassium phosphate, pH 7.6, 0.5 M KCl, 20 mM imidazole, and 10 μM FAD). Thereafter, cells were disrupted by repeated passages in a French press (Gaulin, APV Homogenizer GmbH). Cell debris was separated from the soluble fraction by centrifugation (30 min, 8 °C, 32000*g*), and DNA in the supernatant was digested by DNase I (5 μg/mL DNase, 1 mM $MgCl_2$, 45 min, 8 °C). After an additional centrifugation (30 min, 8 °C, 32000*g*) the clear supernatant was diluted with buffer A to a final volume of 250 mL and applied to a Ni−NTA−agarose column (Qiagen) previously equilibrated with buffer A. The column was washed with 100 mL of buffer A for removal of unspecifically bound proteins. The His_6-tagged protein was eluted using a linear gradient from 0% to 100% buffer B (0.1 M potassium phosphate, pH 7.6, 0.5 M KCl, 0.4 M imidazole) over a total volume of 130 mL. The fractions containing AHAS II were pooled and concentrated by ultrafiltration in centrifugal concentrators with a molecular mass cutoff of 30 kDa (VIVASPIN 15R, 2600*g* and 4 °C). Buffer B was exchanged against buffer C (0.1 M potassium phosphate, pH 7.6, 20 μM FAD) using a HiPrep26/10 desalting column (GE Healthcare Bio-Siences AB) or centrifugal microconcentrators as described above. The purity of the protein was estimated by SDS−PAGE, and the protein concentration was determined by the method of Bradford with BSA as standard (*18*). The proteins were either directly used for functional studies or

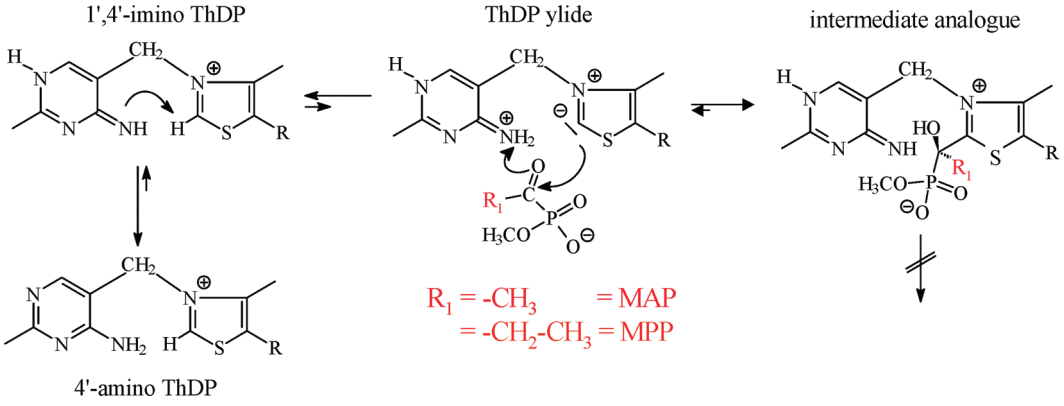

FIGURE 4: Reaction scheme of acyl phosphonate-based substrate analogues with AHAS-bound ThDP. The reaction of MAP or MPP, the phosphonate analogues of pyruvate (MAP) or 2-KB (MPP), with AHAS II leads to the formation of stable predecarboxylation intermediate analogues stabilized in the 1′,4′-imino tautomeric form of the cofactor aminopyrimidine.

stored at −20 °C in 50 mM potassium phosphate buffer, pH 7.6, containing 20 μM FAD, 1 mM DTT, and 50% (v/v) glycerol.

Steady-State Kinetics. The catalytic activity of AHAS was determined in 50 mM potassium phosphate, pH 7.6, 0.2 mM ThDP, 1 mM $MgSO_4$, and 20 μM FAD in two independent assays relying either on the colorimetric detection of the products (*19*, *20*) or on the absorption signal of the substrates, the depletion of which can be directly monitored at 333 nm using an extinction coefficient of 17.5 M^{-1} s^{-1} for pyruvate and of 16.8 M^{-1} s^{-1} for 2-KB (*5*). Kinetic parameters for 2-KB as sole substrate were additionally determined by measuring propiohydroxybutyrate (PHB) formation under the standard conditions using GLC with ECD detection (*21*). The expected degradation product of PHB, 3,4-hexanedione, was used as standard.

The substrate specificity for 2-KB as an acceptor, *R* (*22*), was determined by measuring AHB and AL formation simultaneously in a direct competition experiment with both 2-KB and pyruvate present under standard conditions as given in ref *21*. At a given pyruvate concentration, the total rate of product formation of the two alterative acetohydroxy acids AL and AHB by wild type and some variants of AHAS II is constant (*9*, *17*, *23*), and the 2-KB dependence of the individual rates (V_{AL} and V_{AHB}) can be fitted simultaneously to eqs 1 and 2:

$$V_{AL} = \frac{V[\text{pyruvate}]}{[\text{pyruvate}] + R[\text{2-KB}]} \quad (1)$$

$$V_{AHB} = \frac{VR[\text{2-KB}]}{[\text{pyruvate}] + R[\text{2-KB}]} \quad (2)$$

where [2-KB] is the concentration of 2-KB, and V_{AHB} and V_{AL} are the rates of formation of AHB and AL, respectively. *R* reflects the specificity for 2-KB as acceptor for a given enzyme and is defined by eq 3:

$$R = \frac{V_{AHB}}{V_{AL}}\left(\frac{[\text{pyruvate}]}{[\text{2-KB}]}\right) \quad (3)$$

Thermodynamic Analysis of Donor Substrate Binding by CD Spectroscopy Using Phosphonate-Based Analogues. In order to selectively analyze donor substrate binding, methyl acetylphosphonate (MAP) and methyl propionylphosphonate (MPP) were used as substrate analogues for pyruvate (MAP) and 2-KB (MPP), respectively (Figure 4). These compounds add to C2 of ThDP analogously to 2-keto acids yielding tetrahedral predecarboxylation intermediate analogues, which owing to their stable C2α−P bond do not undergo further processing (*16*). Carbonyl addition of the substrate or analogues to ThDP was shown to be associated with formation of the 1′,4′-imino tautomer of the aminopyrimidine ring that, in the chiral environment of the active site, gives rise to a CD signal centered around 300−310 nm (*24*, *25*).

Prior to the CD titration experiments, 4 mg/mL (corresponding to 58 μM active sites) AHAS II wild type or variants were reconstituted with 1 mM $MgSO_4$ and 0.2 mM ThDP in 50 mM potassium phosphate buffer, pH 7.6, and 20 μM FAD for 10 min at 20 °C. Substrate analogues MAP or MPP were sequentially titrated to the enzyme in a concentration range between 0 and 20 mM (final concentration). After each titration step, binding equilibrium was allowed to establish for 10 min. Subsequently, CD spectra (Jasco J-810 or Applied Photophysics Chirascan spectrapolarimeter) were recorded in the wavelength range of 295−600 nm at 20 °C and using an optical path length of 1 cm. All spectra were corrected for buffer contributions and ongoing dilution in the titration series.

For quantitative analysis, the CD signal at 305 nm was plotted versus analogue concentration. Apparent dissociation constants (K_D^{app}) were calculated by fitting the data to a hyperbolic function or, in case of tight binding, to a quadratic function (eqs 4 and 5) using programs SigmaPlot 11 and KaleidaGraph 3.08.

$$\Theta_{305} = \Theta_{305}{}^{0} + \frac{\Theta_{305}{}^{max}[\text{analogue}]}{K_D{}^{app} + [\text{analogue}]} \quad (4)$$

$$\Theta_{305} = \Theta_{305}{}^{0} + \frac{\Delta\Theta_{305}{}^{max}}{2[\text{AHAS}_0]}\left[([\text{analogue}_0] + [\text{AHAS}_0] + K_D{}^{app}) - \sqrt{([\text{analogue}_0]+[\text{AHAS}_0]+K_D{}^{app})^2 - 4[\text{analogue}_0][\text{AHAS}_0]}\right] \quad (5)$$

where Θ_{305} is the observed CD signal at 305 nm, $\Theta_{305}{}^{0}$ the CD signal of the protein in the absence of substrate analogue, $\Theta_{305}{}^{max}$ the maximum CD signal at substrate analogue saturation, $\Delta\Theta_{305}{}^{max}$ the maximum change of the CD signal at total saturation of enzyme with analogue, and [$analogue_0$] and [$AHAS_0$] the total concentrations of substrate analogue and enzyme, respectively.

Kinetic Analysis of Donor Substrate Binding by Stopped-Flow Absorbance Spectroscopy Using Phosphonate-Based Analogues. The binding kinetics of donor substrate analogues

Table 1: Steady-State Kinetic Constants of AHAS II Wild Type and Variants

reaction measured	parameters	enzyme			
		wild type	V375I	V375A	F109M
2 pyruvate → AL	specific activity (units mg^{-1})	34.3 ± 0.5	22.7 ± 0.4	8.2 ± 0.3	3.4 ± 0.1
	K_M (mM)	6.6 ± 0.4	7.3 ± 0.4	13.8 ± 1.1	17.3 ± 1.6
	k_{cat} (s^{-1})	40.3 ± 0.6	26.6 ± 0.5	9.6 ± 0.4	3.9 ± 0.1
	k_{cat}/K_M (M^{-1} s^{-1})	6100	3650	700	228
	$K_{0.5}$ for ThDP (μM)[a]	0.61 ± 0.18	5.1 ± 0.3	10.4 ± 0.6	1.00 ± 0.08
	K_i for SMM (μM)[b]	1.1 ± 0.1	0.9 ± 0.1	19.6 ± 3.6	17.7 ± 0.5
pyruvate + 2-KB → AL + AHB	R[c]	55.1 ± 3.2	63.6 ± 7.7	56.7 ± 1.9	63.1 ± 2.2
2-KB → PHB	specific activity (units mg^{-1})	2.8 ± 0.9	nad[d]	10.1 ± 0.5	nad[d]
	K_M (mM)	300 ± 122	nad	9.1 ± 1.5	nad
	k_{cat} (s^{-1})	3.3 ± 1.1	nad	11.9 ± 0.6	nad
	k_{cat}/K_M (M^{-1} s^{-1})	11	nad	1308	nad

[a] $K_{0.5}$ is defined as the concentration of ThDP that is required for the half-maximum of AHAS II activity. [b] K_i was determined from the rates of reactions at varied SMM concentrations carried out in the presence of 100 mM pyruvate. [c] R is the substrate specificity for 2-ketobutyrate as the second substrate, (AHB formed)/(AL formed) = R[2-ketobutyrate]/[pyruvate], and was determined by measuring acetohydroxybutyrate and acetolactate formation simultaneously in a competition experiment with varying 2-KB and 50 mM pyruvate in 0.1 M potassium phosphate buffer (pH 7.6) containing 10 mM $MgCl_2$, 0.1 mM ThDP, and 75 μM FAD. [d] No activity detected.

MAP and MPP were analyzed by transient stopped-flow kinetics relying on the absorption signal of the 1′,4′-imino tautomeric form of the resultant covalent intermediate analogues at 310 nm.

Apo-FAD AHAS II (4 mg/mL in 50 mM potassium phosphate buffer, pH 7.6, and 20 μM FAD) was reconstituted with 0.2 mM ThDP and 1 mM Mg^{2+} for 10 min at 37 °C. Thereafter, the enzyme was reacted with defined concentrations of either MAP or MPP (dissolved in same buffer as enzyme, concentration range 0−40 mM) in 1 + 1 mixing ratio at 37 °C using a thermostated SX20 or SX18 stopped-flow spectrophotometer from Applied Photophysics (Leatherhead, U.K.). The reaction was analyzed at 310 nm and using an optical path length of 1 cm. A total of 2000 data points were collected over 1 s. Experiments were carried out in triplicate, and the averaged transients were fitted to a single exponential equation unless otherwise stated using programs SigmaPlot 11 and KaleidaGraph 3.08.

Analysis of Covalent Reaction Intermediates by ^{1}H NMR Spectroscopy after Acid Quench Isolation. In order to estimate unimolecular net rate constants of elementary catalytic steps (see Figure 2), the distribution of enzyme-bound covalent reaction intermediates (LThDP, HEThDP, and AHAThDP) and C2-unsubstituted ThDP at steady state was analyzed by 1D ^{1}H NMR spectroscopy after acid quench isolation as detailed in refs (*8*) and (*26*).

Beforehand, the apo-FAD enzyme (14 mg/mL in 0.1 M potassium phosphate buffer, pH 7.6) was reconstituted with an equimolar amount of ThDP and 1 mM $MgSO_4$ for 10 min at 37 °C. Substrate turnover was then initiated by mixing 200 μL of holo-AHAS with 200 μL of substrate(s) (either 100 mM pyruvate or 50 mM pyruvate + 50 mM 2-KB in the same buffer as enzyme). After a reaction time of 2 s, the reaction was stopped by addition of 200 μL of acidic quench solution (12.5% (w/v) trichloroacetic acid/1 M DCl in D_2O). Denatured protein was discarded after centrifugation. The clear supernatant containing substrate(s), product(s), and intermediates in buffer was further filtrated (0.45 μM pore size) and analyzed by 1D ^{1}H NMR spectroscopy (Bruker Avance 400 NMR spectrometer). The net rate constants of carbonyl addition of pyruvate to ThDP (k'_2; see Figure 2), decarboxylation of LThDP (k'_3), carboligation of HEThDP and acceptor (k'_4), and product liberation (k'_5) steps were calculated on the basis of the relative concentrations of the intermediates. At saturating substrate concentrations, k_{cat} relates to the forward (net) rate constants as follows:

$$\frac{1}{k_{cat}} = \frac{1}{k'_2} + \frac{1}{k'_3} + \frac{1}{k'_4} + \frac{1}{k'_5} \quad (6)$$

At steady state, formation and decay of all intermediates are balanced. Therefore, a direct correlation between the relative concentrations of successive intermediates and corresponding rate constants holds true:

$$\frac{[\mathrm{E-LThDP}]}{[\mathrm{E-ThDP}]} = \frac{k'_2}{k'_3} = a \quad (7)$$

$$\frac{[\mathrm{E-HEThDP}]}{[\mathrm{E-LThDP}]} = \frac{k'_3}{k'_4} = b \quad (8)$$

$$\frac{[\mathrm{E-AHAThDP}]}{[\mathrm{E-HEThDP}]} = \frac{k'_4}{k'_5} = c \quad (9)$$

Substitution of eqs 7−9 into eq 6 then allows to calculate microscopic net rate constants under steady-state turnover conditions:

$$k'_2 = k_{cat}(1 + a + ab + abc) \quad (10)$$

$$k'_3 = k_{cat}\left(\frac{1 + a + ab + abc}{a}\right) \quad (11)$$

$$k'_4 = k_{cat}\left(\frac{1 + a + ab + abc}{ab}\right) \quad (12)$$

$$k'_5 = k_{cat}\left(\frac{1 + a + ab + abc}{abc}\right) \quad (13)$$

RESULTS

Steady-State Kinetic Analysis of Val375 and Phe109 Variants. Substrate turnover (2 pyruvate → AL) was analyzed under steady-state conditions for AHAS II variants Val375Ile, Val375Ala, and Phe109Met, and the macroscopic kinetic constants

are summarized in Table 1. While the Val375Ile variant exhibits steady-state kinetic parameters similar to those of wild-type AHAS II with only a slight reduction of k_{cat} but virtually unchanged K_M for pyruvate, variant Val375Ala has a 4-fold compromised k_{cat} along with a 2-fold increase of the Michaelis constant resulting in an overall ~10-fold reduction of the catalytic efficiency (k_{cat}/K_M) for AL formation (wt, 6100 M^{-1} s^{-1}; Val375Ala, 700 M^{-1} s^{-1}). Variant Phe109Met shows a ~10-fold reduction in k_{cat} and a 3-fold increase of K_M and thus exhibits the lowest catalytic efficiency of all variants in this study (228 M^{-1} s^{-1}).

Competition experiments in the presence of the alternative acceptors pyruvate and 2-KB (*21*) revealed that the high preference for 2-KB over pyruvate as acceptor seen for the wild type ($R \sim 55$) is retained in all variants such that formation of AHB (pyruvate + 2-KB → AHB) is heavily favored over AL production.

The nonphysiological condensation of two 2-KB molecules (product PHB) is poorly catalyzed by AHAS II wild type with a catalytic efficiency (11 M^{-1} s^{-1}) almost 2 orders of magnitude lower than that of AL or AHB formation, resulting from both lower turnover numbers and reduced substrate affinity. Since 2-KB is the preferred physiological acceptor, this result indicates 2-KB to be only weakly bound and converted as donor. Remarkably, the catalytic efficiency for PHB formation of the Val375Ala variant, in which the donor substituent subsite is enlarged and thus expected to better accommodate 2-keto acid substrates larger than pyruvate, is 100-fold increased (1308 M^{-1} s^{-1}) compared to wild-type AHAS II (11 M^{-1} s^{-1}) as a consequence of 3-fold increased k_{cat} and 30-fold lowered substrate Michaelis constant. Even more intriguing, the catalytic efficiency of Val375Ala for PHB formation exceeds its efficiency for condensation of pyruvate as donor with either pyruvate or 2-KB as acceptor (700 M^{-1} s^{-1}), prompting us to conclude that the donor preference has been inverted in the variant, which, contrary to the wild type, favors 2-KB over pyruvate as donor.

Notably, a substitution of Val375 by Ile or Ala clearly affects ThDP binding of AHAS under turnover conditions as evidenced by the 10-fold (Val375Ile) or 20-fold (Val375Ala) increase of $K_{0.5}$ (ThDP). While the K_i for binding of the inhibitor sulfometuron methyl (SMM) is almost unchanged in Val375Ile relative to the wild type, a 20-fold decrase in affinity is observed for variant Val375Ala. In variant Phe109Met, cofactor binding is not affected, but the K_i for inhibitor SMM is increased. Interestingly, although no published structures of herbicide−AHAS complexes show contacts with the homologous Val or Phe residues, we do observe altered herbicide binding in the variants.

Thermodynamic Analysis of Donor Substrate Binding by CD Spectroscopy. Although the steady-state kinetic analysis of Val375 and Phe109 variants provided ample evidence for the general involvement of the two side chains in donor substrate binding, we aimed at selectively analyzing the donor binding sequence by employing acylphosphonates as donor substrate analogues. In that way it is possible to single out all catalytic steps encompassing formation of the substrate Michaelis complex and of the covalent donor−ThDP adduct (Figure 4). X-ray crystallographic studies on several ThDP-dependent enzymes including POX and pyruvate dehydrogenase demonstrated that these analogues bind in a similar fashion as the native 2-keto acid substrates (*13*, *27*, *28*). Further, it could be demonstrated that the aminopyrimidine moiety of the enzyme-bound cofactor gives rise to both absorbance and CD signals, which can be used as a selective spectroscopic probe to assess the tautomeric and ionization state of the aminopyrimidine. In the case of C2α-tetrahedral

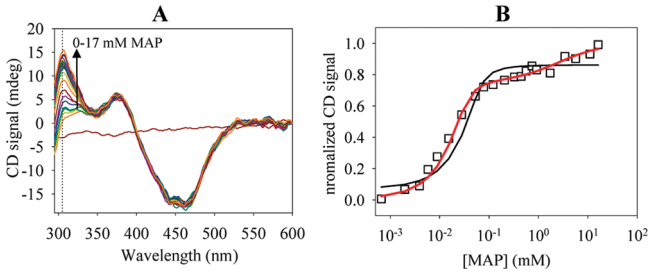

FIGURE 5: Formation of the stable LThDP analogue 1′,4′-imino-2α-phosphonolactyl-ThDP in AHAS II after reaction of the enzyme with pyruvate analogue MAP as detected by CD spectroscopy. (A) Circular dichroism spectra obtained after addition of increasing amounts of MAP (0−17 mM) to 58 μM holo-AHAS II wild type in 0.05 M potassium phosphate, pH 7.6 at 20 °C. (B) The dependence of the CD signal intensity at 305 nm on the MAP concentration was fitted to either a quadratic equation (black fit) or an equation with two quadratic terms (red fit), the latter accounting for a putative half-of-the-sites reactivity of AHAS. Fitting the data yielded a dissociation constant of either 4.2 ± 3.4 μM (black fit, P value = 0.23, R^2 = 0.94) or 2.7 ± 1.4 μM (red fit, P value = 0.07, R^2 = 0.99) and thus favors a mechanism that includes half-of-the-sites reactivity.

intermediates such as the covalent acylphosphonate−ThDP adduct, ThDP enzymes preferentially stabilize the 1′,4′-imino tautomeric form which gives rise to a CD signal between 300 and 310 nm (*24*). In line with these precedents, the addition of either the pyruvate analogue MAP or the 2-KB analogue MPP to AHAS II wild type and Val375/Phe109 variants induced changes in the 300−310 nm range of the CD spectra indicating a change in the protonation state of ThDP, i.e., formation of the imino tautomer (Figure 5A). The region between 350 and 500 nm, which corresponds to the enzyme-bound FAD cofactor, remains unchanged. Quantitative analysis of the CD data at 305 nm revealed that assuming a single binding equilibrium is not sufficient to adequately fit the data of wild-type AHAS II (black fit in Figure 5B) because the binding isotherm consists of a high-affinity and a low-affinity branch. We therefore fitted the data according to a model in which we included chemical nonequivalence between the two active sites in the functional AHAS dimer. This assumption is based on recent structural and functional studies on numerous ThDP enzymes, which indicated negative cooperativity or even half-of-the-sites reactivity in these enzymes (*29*−*31*). Fitting of the CD titration data using a function with two identical quadratic terms each accounting for half of the active sites revealed a K_D of 2.7 ± 1.4 μM for the high-affinity site, whereas the dissociation constant is 3 orders of magnitude larger for the low-affinity site (K_D = 2.6 mM) (red fit in Figure 5B). Notably, this chemical nonequivalence could not be observed for any of the mutants or for the reaction of AHAS with the 2-KB analogue MPP. In this regard, the origins of the different kinetic behavior of wild-type AHAS and the single site variants remain to be elucidated.

Any substitution of Val375 or Phe109 decreased the affinity of AHAS II for MAP 10−100-fold (Figure 6A and Table 2). This effect is least pronounced in variant Val375Ala (K_D = 32.5 ± 8.3 μM), whereas Val375Ile (K_D = 151 ± 35 μM) and Phe109Met (K_D = 175 ± 29 μM) variants are greatly impaired in binding the pyruvate analogue.

A different outcome is observed for the thermodynamic analysis of MPP (2-KB analogue) binding (Figure 6B and Table 2). The wild-type enzyme shows a 160-fold reduced affinity for MPP (K_D = 434 ± 49 μM) compared to MAP binding (K_D = 2.7 ± 1.4 μM). The Val375Ala protein binds MPP with the highest affinity (K_D = 10.2 ± 1.7 μM) of all proteins tested and

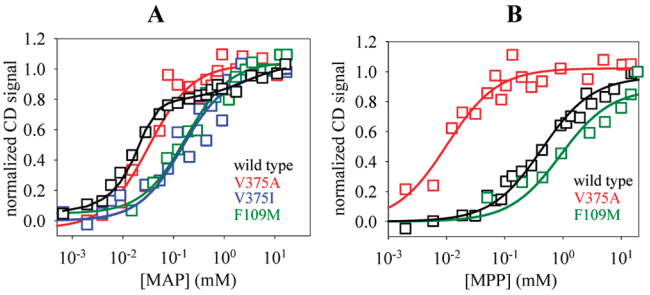

FIGURE 6: Thermodynamic analysis of MAP (A) and MPP (B) binding to AHAS II wild type and variants (Val375Ala, Val375Ile, Phe109Met) using CD spectroscopy. The dependence of the normalized CD signals at 305 nm was fitted to hyperbolic or quadratic equations. The corresponding dissociation constants are summarized in Table 2.

exhibits a 3-fold preference for MPP over MAP. Amazingly, the variant exhibits a similar affinity for MPP as wild type for MAP. The Val375Ile variant fails to bind the 2-KB analogue, and the Phe109Met variant shows a 100-fold compromised K_D^{app} relative to Val375Ala.

Kinetic Analysis of Donor Substrate Binding by Stopped-Flow Spectroscopy. Kinetics of donor substrate binding was analyzed by stopped-flow absorption spectroscopy at 310 nm using the intrinsic absorbance of the cofactor 1′,4′-imino tautomer which is stabilized upon formation of the covalent acylphosphonate−ThDP adduct. The stopped-flow transients recorded after mixing of wild-type AHAS with different MAP concentrations (Figure 7A) were fitted to a single exponential function. Plotting of the derived rate constants versus the MAP concentration employed revealed a hyperbolic dependence of k_{obs} implying a reversible two-step mechanism with transient formation of a Michaelis complex as a preceding rapid equilibrium.

$$\text{E}-\text{ThDP} + \text{analogue} \underset{}{\overset{K_1}{\rightleftharpoons}} \text{E}-\text{ThDP}*\text{analogue (Michaelis complex)} \quad (14)$$

$$\text{E}-\text{ThDP}*\text{analogue} \underset{k_{-2}}{\overset{k_{+2}}{\rightleftharpoons}} \text{E}-\text{analogue}-\text{ThDP (covalent adduct)} \quad (15)$$

The dependence of k_{obs} on the phosphonate (MAP or MPP) concentration was fitted according to eq 16:

$$k_{obs} = k_{-2} + \frac{k_{+2}[\text{analogue}]}{K_1 + [\text{analogue}]} \quad (16)$$

where k_{+2} and k_{-2} are the unimolecular rate constants of carbonyl addition and elimination and K_1 is the dissociation constant of the preequilibrium. In some instances (reaction of variants Val375Ala and Phe109Met with MPP), a linear dependence of k_{obs} versus the analogue concentrations employed was observed. Such a kinetic behavior can be expected when the employed analogue concentrations are not saturating (K_1 > [analogue]). In this case, k_{obs} values were fitted according to eq 17.

$$k_{obs} = k_{-2} + \frac{k_{+2}}{K_1}[\text{analogue}] \quad (17)$$

The rate constants derived for the reaction of wild-type AHAS II with both MAP and MPP exhibit a hyperbolic dependence on the analogue concentration (Figure 7B,C) and were fitted according to eq 16. While elimination of the analogues from the covalent

Table 2: Thermodynamic and Kinetic Analysis of MAP (Phosphonate Analogue of Pyruvate) and MPP (Phosphonate Analogue of 2-KB) Binding to AHAS II Wild Type and Variants

	enzyme			
parameters	wild type	V375I	V375A	F109M
CD titration[a]				
K_D^{app}(MAP) (μM)	2.7 ± 1.4	151 ± 35	32.5 ± 8.3	175 ± 29
K_D^{app}(MPP) (μM)	434 ± 49	nbd[c]	10.2 ± 1.7	910 ± 290
kinetics of MAP binding[b]				
K_1 (mM)	5.0 ± 1.3	5.6 ± 1.1	20 ± 12	29 ± 25
k_{+2} (s^{-1})	180 ± 17	116 ± 6	118 ± 37	39 ± 15
k_{-2} (s^{-1})	1.8 ± 1.2	4.5 ± 2.9	1.8 ± 1.1	2.4 ± 1.1
kinetics of MPP binding[b]				
K_1 (mM)	15.6 ± 7.9	nbd[c]	nd[d]	nd[d]
k_{+2} (s^{-1})	28 ± 6	nbd[c]	nd[d]	nd[d]
k_{-2} (s^{-1})	1.7 ± 1.0	nbd[c]	1.9 ± 1.3	10.4 ± 1.5
k_{+2}/K_1 (s^{-1} mM^{-1})	1.8	nbd[c]	11.8 ± 1.3	0.53 ± 0.12

[a]At 20 °C. [b]At 37 °C. [c]No binding detectable. [d]Not determined. Since a linear dependence of k_{obs} on the analogue concentration was observed, K_1 and k_{+2} cannot be estimated independently but rather their ratio (k_{+2}/K_1). For wild-type enzyme, k_{+2} and K_1 were estimated independently.

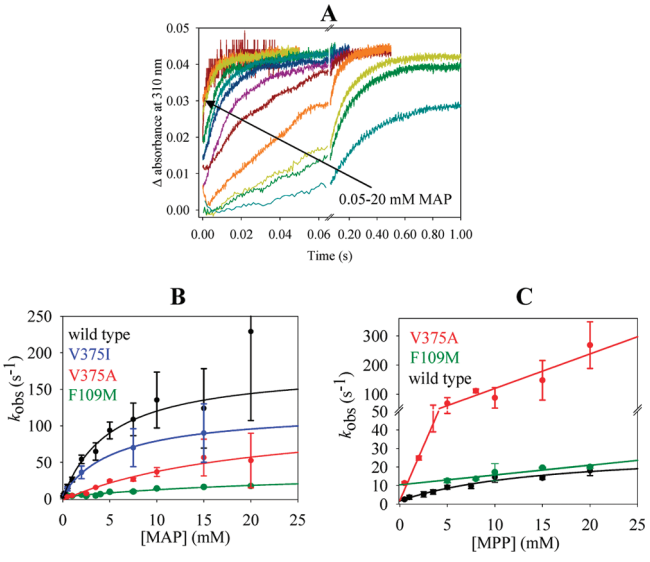

FIGURE 7: Stopped-flow kinetic analysis of MAP and MPP binding to AHAS II wild type and variants. (A) Stopped-flow transients at 310 nm after reaction of AHAS II wild type with increasing concentrations of MAP at 37 °C. Reaction conditions are given in the Materials and Methods section. (B) Dependence of the observed rate constants on MAP concentration for AHAS II wild type (black) and variants Val375Ile (blue), Val375Ala (red), and Phe109Met (green). Data were fitted to eq 16, and the resultant rate and dissociation constants are summarized in Table 2. (C) Dependence of the observed rate constants on MPP concentration for AHAS II wild type (black) and variants Val375Ala (red) and Phe109Met (green). Data were fitted to either eq 16 (wild-type AHAS) or eq 17 (Val375Ala and Phe109Met), and the resultant rate and dissociation constants are summarized in Table 2.

analogue−ThDP conjugates (k_{-2}) has comparable rate constants of approximately 2 s^{-1}, the unimolecular rate constant of carbonyl addition (k_{+2}) at saturating analogue concentrations is 6-fold higher for the pyruvate analogue MAP (~180 s^{-1}) versus the 2-KB analogue MPP (~30 s^{-1}). Also, the wild-type enzyme exhibits a 3-fold higher affinity for MAP (K_1 ~ 5 mM) versus MPP (K_1 ~ 16 mM) regarding the preequilibrium and formation of the Michaelis complex.

All variants tested in this study are kinetically and thermodynamically impaired in their ability to bind MAP with the Phe109Met variant showing the most dramatic effects. The latter protein has a 6-fold increased K_I value (~30 mM) along with a 4−5-fold reduced rate constant of analogue addition to C2 of enzyme-bound ThDP at saturating analogue concentrations. Both the Val375Ala and Val375Ile variants show approximately 2-fold reduced k_{+2} values and, in the case of the former protein, a 4-fold increased K_I dissociation constant. When the variants were reacted with 2-KB analogue MPP, variant Val375Ala could be demonstrated to bind the analogue with higher rate constants than the wild type over the whole concentration range tested. The observed rate constants were found to be linearly dependent on the MPP concentration until 20 mM analogue ($k_{+2}/K_I \sim 12\,mM^{-1}\,s^{-1}$), consistent with nonsaturation of the protein under these conditions. At 20 mM, k_{obs} of MPP binding in the Val375Ala variant (~300 s^{-1}) is approximately 10 times higher than in wild-type AHAS. Despite a dramatically increased affinity for MPP (K_D^{app}) compared to wild type in the CD spectroscopic analysis, Val375Ala does not show a hyperbolic dependence in the kinetic experiments, indicating that the altered binding thermodynamics almost entirely result from changes of K_2 (k_{-2}/k_{+2}) that is reversible formation of the covalent pre-decarboxylation intermediate, whereas a stronger reactant state stabilization of the substrate Michaelis complex cannot account for the observed effects. Variant Phe109Met also exhibits a linear dependence of k_{obs} versus the MPP concentration employed, although the slope ($k_{+2}/K_I \sim 0.5\ mM^{-1}\ s^{-1}$) is significantly smaller than observed for Val375Ala. The unimolecular dissociation of MPP from the covalent adduct has the highest rate constant ($k_{-2} \sim 10\ s^{-1}$) of all proteins tested.

It has to be noted that the K_D^{app} values calculated on the basis of the kinetic experiments

$$K_D^{app} = \frac{K_1 K_2}{1 + K_2} \tag{18}$$

with

$$K_2 = k_{-2}/k_{+2} \tag{19}$$

do not match the dissociation constants obtained in the CD titration experiments for some proteins. This apparent discrepancy might result from the fact that stopped-flow binding kinetics were conducted in the subsecond time regime, where binding in only the fast-binding active site is observed, whereas slow binding of MAP or MPP in the "dormant site" is negligible (data not shown).

NMR-Based Analysis of ThDP Intermediates at Steady State. The quantitative distribution of reaction intermediates (C2-unsubstituted ThDP, LThDP, HEThDP, and ALThDP) in AHAS turning over substrate at steady state can be analyzed by ^{1}H NMR spectroscopy after acid quench isolation. Our previous studies on AHAS II wild type had revealed that at saturating substrate concentrations the unimolecular carbonyl addition of bound pyruvate to C2 of ThDP is overwhelmingly rate-determining, whereas all other catalytic steps such as decarboxylation of LThDP and condensation of HETHDP enamine and acceptor as well as product liberation proceed at least 1 order of magnitude faster, as evidenced by the predominant accumulation of C2-unsubstituted ThDP and of only small fractions of all other intermediates (*8*, *26*).

When using pyruvate as the sole substrate (2 pyruvate → AL), C2-unsubstituted ThDP and the covalent product−ThDP adduct (ALThDP) are accumulated at steady state in variant Val375Ala to ~75% (ThDP) and ~25% (ALThDP) occupancy, indicating that both donor binding and product release are partially rate-determining (Figure 8). A comparison of the derived net rate constants with those of the wild-type enzyme shows that these elementary steps (donor binding and product release) are compromised by severalfold in the variant (Table 3). The data do not suggest that decarboxylation of LThDP or carboligation of the acceptor is affected in Val375Ala AHAS II. As opposed to these findings, NMR analysis of Val375Ile indicates donor binding and, to a lesser degree, decarboxylation of LThDP to be impaired with no detectable impact on the acceptor half-reaction (that is, carboligation and product liberation). Variant Phe109Met is deficient in multiple steps of catalysis including LThDP formation, decarboxylation of the latter, and product release as evidenced by 10-fold decreased microscopic rate constants (Table 3).

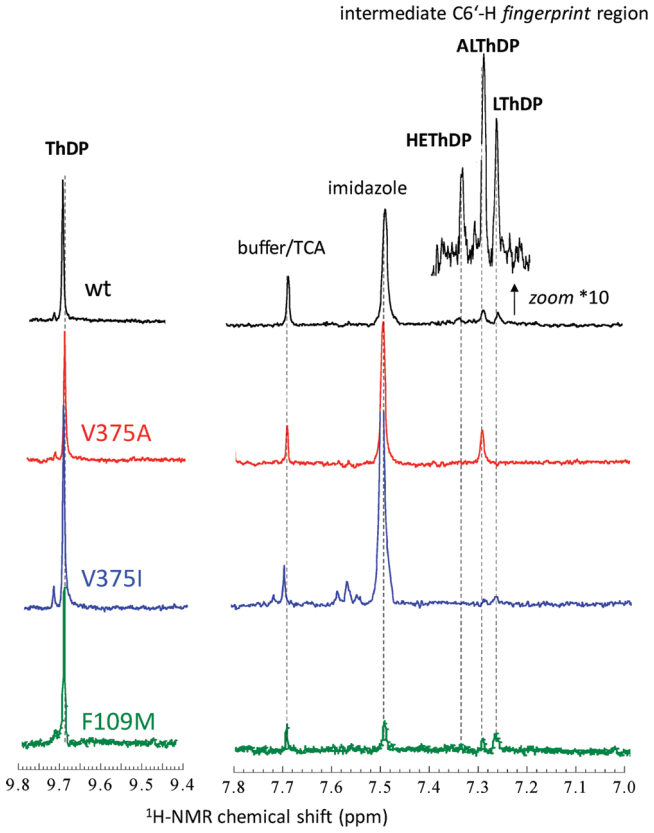

FIGURE 8: Detection and quantitation of covalent intermediates in the reactions of AHAS II wild type (black) and variants Val375Ala (red), Val375Ile (blue), and Phe109Met (green). Steady-state intermediate distribution of AHAS II in the presence of 100 mM pyruvate in 0.1 M potassium phosphate, pH 7.6 at 37 °C. Reactions were quenched after 2 s, and the protein-free solutions obtained after centrifugation were analyzed by 1D ^{1}H NMR spectroscopy at 300 K. Exemplified for the wild-type protein, the C6′-H intermediate fingerprint region (7.0−7.8 ppm) is zoomed 10-fold relative to the downfield region where the C2-H signal of C2-unsubstituted ThDP appears.

When AHAS Val375 and Phe109 variants are reacted with pyruvate and 2-KB (product AHB), only very minor fractions of covalent intermediates can be detected, paralleling the results obtained with the wild type and showing similar kinetic significances of elementary catalytic steps under steady-state turnover conditions.

Table 3: Microscopic Rate Constants for Elementary Steps in the Reactions of Wild-Type AHAS II and Variants[a]

enzyme	reaction[b]	k_{cat} (s^{-1})	k'_2 (s^{-1})	k'_3 (s^{-1})	k'_4 (s^{-1})	k'_5 (s^{-1})
wild type[c]	Pyr + Pyr	40	~48	~1000	~2100	~350
	Pyr + 2-KB	40	~42	~800	> 4000	> 4000
Val375Ala	Pyr + Pyr	10	~13	> 500[d]	> 500	~50
	Pyr + 2-KB	10	~10	> 500	> 500	> 500
Val375Ile	Pyr + Pyr	27	~28	~600	> 600	> 600
	Pyr + 2-KB	27	~28	~670	> 1300	> 1300
Phe109Met	Pyr + Pyr	4	~5	~45	> 130	~65
	Pyr + 2-KB	13	~15	~150	> 300	> 300

[a]Net rate constants (see Figure 2) for formation of LThDP from bound pyruvate (k'_2), decarboxylation of LThDP (k'_3), covalent ligation of the second keto acid (k'_4), and release of acetohydroxy acid product (k'_5) were calculated using eqs 6−13, from k_{cat} and the distribution of ThDP-bound intermediates, determined by the rapid mixing-quench/NMR method at 37 °C in 0.1 M potassium phosphate, pH 7.6. The major source of error in the analysis of the distribution of intermediates is the error in the integration of the individual signals of the intermediate species, and it is therefore dependent on the signal-to-noise ratio of the respective signals. Typically, the error varied between approximately 10% and 20%, the latter value being relevant for poorly resolved signals. [b]Pyr + Pyr is the formation of acetolactate from two molecules of pyruvate in the presence of 100 mM pyruvate. Pyr + 2-KB is the formation of acetohydroxybutyrate from pyruvate and 2-ketobutyrate in the presence of 50 mM each. Under these conditions, less than 2% of the reaction catalyzed by the wild-type enzyme and variants goes to acetolactate. [c]The specific activity of wild-type AHAS II used in this study is higher than previously reported. The quantitative distribution of reaction intermediates, however, could be reproduced within experimental error and thus results in higher net rate constants with no change of their relative ratio. [d]Lower limits of rate constants reflect a limit of resolvability of the ^{1}H NMR spectra (signal-to-noise ratio = 3).

DISCUSSION

AHASs belong to a family of enzymes that use the bioorganic cofactor ThDP as the biologically active form vitamin B_1. Structural studies on ThDP enzymes have identified a canonical cofactor binding mode in which the cofactor adopts the so-called "V conformation" that is characterized by a V-shaped orientation of the thiazolium and aminopyrimidine rings bridged via a methylene group (*32*). In this conformation, the reactive C2 atom of the thiazolium ring and the exocyclic 4′-amino group of the aminopyrimidine are juxtaposed, enabling the latter to function as an intramolecular acid/base catalyst for cofactor activation (C2 deprotonation) as well as for carbonyl addition/elimination of substrates and products, respectively. Besides the conserved cofactor binding mode, the stereochemical course of substrate binding and processing appears, on the basis of the currently available data, to also be a conserved feature in the ThDP enzyme family (*28*). The X-ray structural analysis of reaction intermediates and intermediate analogues trapped in the active centers of ThDP enzymes indicated a conserved absolute configuration C2α stereocenter of the intermediates (the carbonyl carbon of the substrate) resulting from a common three-center binding mode with specific interactions for the substrate leaving group, the substrate carbonyl, and the substrate substituent. Accordingly, the scissile substrate bond connecting C2α and the leaving group moiety (e.g., the carboxylate in the case of 2-keto acid substrates) is always directed perpendicular to the thiazolium ring plane, the C2α-OH is placed in close proximity to the 4′-amino group of the aminopyrimidine, and the substrate substituent is accommodated in a specific "substitutent pocket" (*14*, *28*). Sequence alignments and structural analysis of ThDP enzymes belonging to the POX subfamily that includes POX, AHAS, GCL, and other FAD-containing enzymes reveal that the substrate-derived substituent is bound to a hydrophobic patch constituted by the flavin isoalloxazine, a conserved Phe, and either a Val (pyruvate-processing enzymes) or Ile residue (glyoxylate-processing GCL) (Figure 3) (*10*, *15*, *33*, *34*). Since the substrate substituent of glyoxylate (−H) is smaller than that of pyruvate ($-CH_3$), it is tempting to speculate that the Val or Ile residue in question confers specificity for the corresponding native substrate by a combination of sterically and hydrophobically controlled substrate binding in terms of shape complementarity. This appears to be a universal principle in ThDP enzymes and is not solely restricted to the POX subfamily; other ThDP enzymes acting on pyruvate also contain either a Val (1-deoxy-D-xylulose 5-phosphate synthase, DXS; bacterial pyruvate dehydrogenase E1 component, PDH-E1) or an isosteric (although more polar) Thr residue (pyruvate decarboxylase, PDC; pyruvate:ferredoxin oxidoreductase, PFOR), all of which are located at the *si*-face of the ThDP thiazolium nucleus (*35*−*39*). In ThDP enzymes that process 2-keto acids with larger substrate substituents (benzoylformate decarboxylase, BFDC; benzaldehyde lyase, BAL), the specificity pocket is wider and consists of several aromatic residues, between which the substrate phenyl substituent is sandwiched as revealed by crystallographic snapshots of intermediate analogues after cocrystallization of these enzymes with substrate analogues benzoylphosphonate or methyl benzoylphosphonate (*40*−*42*). In ThDP enzymes that catalyze conversion of sugar substrates bearing hydroxymethyl substituents rather than a methyl group (transketolase, TK), a His is located in a comparable position to the Val or Thr in pyruvate-processing enzymes (*43*, *44*).

Here, we have examined the functional roles in substrate binding and substrate specificity of the conserved Val and Phe residues (Val375 and Phe109) belonging to the donor substrate substituent pocket in AHAS II from *E. coli*. A special trait of AHASs that separates them from many other ThDP enzymes is that they convert two identical or highly similar substrate molecules by condensing pyruvate (donor substrate) with either another pyruvate or, alternatively, 2-KB as the first committed step in BCAA biosynthesis. Whereas most AHASs exhibit a high preference for 2-KB over pyruvate as acceptor, which ensures a balanced formation of all BCAAs because the intracellular concentrations of 2-KB are almost 2 orders of magnitude lower than of pyruvate, the sole physiological donor in all AHASs is pyruvate. Our previous studies (*9*) could provide evidence that a tryptophan residue in the acceptor pocket (Trp464 in AHAS II) is a critical determinant that mediates preferential binding of 2-KB as a consequence of stronger hydrophobic interactions of its indole side chain with the (CH_3-CH_2-) substituent of 2-KB versus ($-CH_3$) of pyruvate. Our analogous studies on the donor substrate pocket now reveal that steric hindrance and unfavorable orbital alignment of reaction intermediates impede binding and conversion of 2-KB as donor in AHAS, with Val375 as a key component. The steady-state kinetic analysis of Val375 variants showed that a smaller side chain at this position leads to a change of the donor substrate preference (Table 1). While wild-type AHAS II is a very poor catalyst for the nonphysiological condensation of two 2-KB molecules to give PHB as product, with a k_{cat}/K_M of 11 M^{-1} s^{-1} several orders of magnitude lower than those for the physiological reactions with pyruvate as donor (6100 M^{-1} s^{-1}), the catalytic efficiency for the carboligation of 2-KB as donor and acceptor in Val375Ala variant is increased over 100-fold (1300 M^{-1} s^{-1}). This increase compared to wild-type AHAS results from both increased substrate affinity (lower

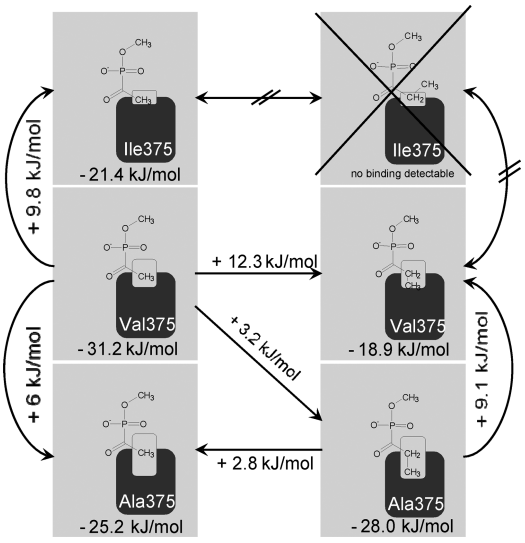

FIGURE 9: Scheme showing the free energies of MAP and MPP binding (ΔG_b) in AHAS II wild type and variants under each cartoon and the resultant differences ($\Delta\Delta G_b$) between the individual proteins. A thermodynamic standard state of 1 M was used for calculation of binding energies.

K_M) and higher turnover (k_{cat}). Intriguingly, when relating to catalytic efficiency, the variant favors formation of propiohydroxy acids (2-KB as donor) ~2-fold over formation of the physiological acetohydroxy acid products (pyruvate as donor). As expected, a replacement of Val375 by the bulkier Ile residue abrogated the ability of AHAS II to catalyze the condensation of two 2-KB molecules, whereas moderate effects were observed for the physiological reactions (AL and AHB formation). Residue Phe109 appears to play a more general role for donor substrate binding, as its replacement by the less hydrophobic Met side chain had strong effects on k_{cat} and K_M. Both Val375 and Phe109 seem to be exclusively involved in donor binding and/or interactions with donor-derived moieties of intermediates because the high preference for 2-KB as acceptor is preserved (Table 1).

In order to selectively analyze binding of the donor substrate in the absence of acceptor and without turnover, we have chemically synthesized acylphosphonates bearing either a methyl substituent (MAP) or an ethyl substituent (MPP) as analogues of pyruvate and 2-KB. Acylphosphonates bind to C2 of enzyme-bound ThDP but will not be further processed. The binding of MAP and MPP to AHAS II wild type and Val375/Phe109 variants was analyzed by circular dichroism spectroscopy under equilibrium conditions and by stopped-flow kinetics. The thermodynamic analysis by CD spectroscopy revealed that AHAS wild type displays half-of-the-sites reactivity as was demonstrated quite recently as well for numerous related ThDP-dependent enzymes such as pyruvate dehydrogenase (*45*). The overall dissociation constant for MAP as the pyruvate analogue is 2.7 μM in wild-type AHAS II, and any mutation at position Val375 or Phe109 leads to a multifold decrease in affinity with Val375Ile and Phe109Met showing the most dramatic effects (K_M^{app} ~150 and ~175 μM), whereas Val375Ala exhibits only a 10-fold reduced affinity. The dissociation constant of the wild-type enzyme for the 2-KB analogue MPP (K_M^{app} ~ 430 μM) is 2 orders of magnitude higher than that of MAP which translates into more than 12 kJ/mol less binding energy (Figure 9). In the Val375Ala variant, MPP is bound with an affinity (K_M^{app} ~ 10 μM) comparable to the binding of MAP by wild-type AHAS (K_M^{app} ~ 3 μM). Furthermore, the Val375Ala variant exhibits a 3-fold higher affinity for MPP over MAP, which is an equivalent of 2.8 kJ/mol $\Delta\Delta G_b$ and reflects the expected differences in hydrophobicity between a methyl and an ethyl group. A reduction of the size of the substrate substituent pocket (Val375Ile) abrogates the ability of AHAS to bind MPP. The Phe109Met variant showed poor affinity for both MAP and MPP with a 5-fold preference for the pyruvate analogue pointing to an important role of Phe109 for holding the substrate in the active site by hydrophobic interactions. The kinetic analysis of MAP and MPP binding by stopped flow leads to a result similar to that of the thermodynamic analysis and supports the functional assignments of Val375 and Phe109 for substrate binding and specificity. The kinetic analysis further revealed that the substrate analogues bind to enzyme-bound ThDP in a two-step reversible mechanism with transient formation of a noncovalent complex, i.e., the Michaelis complex, paralleling the results on benzoylformate decarboxylase (*41*). A substitution of Val375 or Phe109 affected both formation of the Michealis complex (K_1 in Table 2) and of the covalent adduct (k_{+2} in Table 2), clearly demonstrating that the interactions of the two side chains are not only required to lure the donor substrate into the active site and to sterically hinder 2-KB but moreover correctly orient the substrate in the docking site prior to carbonyl addition to C2 of ThDP. This proposed function is further supported by the NMR-based intermediate analysis at steady state, which indicated that formation of LThDP from bound pyruvate is affected in all variants although (almost) saturating substrate concentrations were employed (Figure 8 and Table 3). Moreover, it becomes evident that a mutation of either Val375 or Phe109 not only affects initial substrate binding and subsequent carbonyl addition to ThDP but additionally impairs elementary catalytic steps in which intermediates with tetrahedral C2α are involved, such as decarboxylation of LThDP and product liberation from the covalent product−ThDP (AHAThDP in Figure 2) adduct. In Val375Ala and Phe109Met variants, the net rate constants of product release are ~10-fold decreased compared to the wild-type enzyme (Table 3). The Phe109Met variant is additionally deficient in catalyzing the decarboxylation of LThDP as evidenced by an ~20-fold smaller k'_3.

CONCLUSIONS

ThDP-dependent enzymes share a common three-center substrate binding mode, in which the substrate substituent accommodates in a specific shape-complementary pocket. In most ThDP enzymes that act on pyruvate, a Val or Thr residue is supposed to interact with the methyl group of pyruvate and of cofactor intermediates derived from it. As exemplified here for AHAS II, this residue is a critical determinant for conferring substrate specificity as it sterically hinders 2-keto acids larger than pyruvate binding to ThDP. The interaction between the Val or Thr side chain and the substrate methyl substituent is further important for the correct orientation of tetrahedral intermediates and their innate reactivity. A Phe residue found to be conserved among the POX subfamily provides more than 10 kJ/mol binding energy by hydrophobic interaction of its phenyl ring with the substrate CH_3 substituent.

REFERENCES

1. Chipman, D., Barak, Z. A., and Schloss, J. V. (1998) Biosynthesis of 2-aceto-2-hydroxy acids: acetolactate synthases and acetohydroxyacid synthases. *Biochim. Biophys. Acta 1385*, 401–419.
2. Chipman, D. M., Duggleby, R. G., and Tittmann, K. (2005) Mechanisms of acetohydroxyacid synthases. *Curr. Opin. Chem. Biol. 9*, 475–481.
3. McCourt, J. A., and Duggleby, R. G. (2006) Acetohydroxyacid synthase and its role in the biosynthetic pathway for branched-chain amino acids. *Amino Acids 31*, 173–210.
4. Chang, Y. Y., and Cronan, J. E. (1988) Common ancestry of *Escherichia coli* pyruvate oxidase and the acetohydroxy acid synthases of the branched-chain amino acid biosynthetic pathway. *J. Bacteriol. 170*, 3937–3945.
5. Tittmann, K., Schröder, K., Golbik, R., McCourt, J., Kaplun, A., Duggleby, R. G., Barak, Z., Chipman, D. M., and Hübner, G. (2004) Electron transfer in acetohydroxy acid synthase as a side reaction of catalysis. Implications for the reactivity and partitioning of the carbanion/enamine form of (alpha-hydroxyethyl)thiamin diphosphate in a "nonredox" flavoenzyme. *Biochemistry 43*, 8652–8661.
6. Gollop, N., Damri, B., Chipman, D. M., and Barak, Z. (1990) Physiological implications of the substrate specificities of acetohydroxy acid synthases from varied organisms. *J. Bacteriol. 172*, 3444–3449.
7. Vinogradov, V., Vyazmensky, M., Engel, S., Belenky, I., Kaplun, A., Kryukov, O., Barak, Z., and Chipman, D. M. (2006) Acetohydroxyacid synthase isozyme I from *Escherichia coli* has unique catalytic and regulatory properties. *Biochim. Biophys. Acta 1760*, 356–363.
8. Tittmann, K., Vyazmensky, M., Hübner, G., Barak, Z., and Chipman, D. M. (2005) The carboligation reaction of acetohydroxyacid synthase II: Steady-state intermediate distributions in wild type and mutants by NMR. *Proc. Natl. Acad. Sci. U.S.A. 102*, 553–558.
9. Ibdah, M., BarIlan, A., Livnah, O., Schloss, J. V., Barak, Z., and Chipman, D. M. (1996) Homology modeling of the structure of bacterial acetohydroxy acid synthase and examination of the active site by site-directed mutagenesis. *Biochemistry 35*, 16282–16291.
10. Pang, S. S., Duggleby, R. G., and Guddat, L. W. (2002) Crystal structure of yeast acetohydroxyacid synthase: A target for herbicidal inhibitors. *J. Mol. Biol. 317*, 249–262.
11. McCourt, J. A., Pang, S. S., Guddat, L. W., and Duggleby, R. G. (2005) Elucidating the specificity of binding of sulfonylurea herbicides to acetohydroxyacid synthase. *Biochemistry 44*, 2330–2338.
12. McCourt, J. A., Pang, S. S., King-Scott, J., Guddat, L. W., and Duggleby, R. G. (2006) Herbicide-binding sites revealed in the structure of plant acetohydroxyacid synthase. *Proc. Natl. Acad. Sci. U.S.A. 103*, 569–573.
13. Wille, G., Meyer, D., Steinmetz, A., Hinze, E., Golbik, R., and Tittmann, K. (2006) The catalytic cycle of a thiamin diphosphate enzyme examined by cryocrystallography. *Nat. Chem. Biol. 2*, 324–328.
14. Tittmann, K., and Wille, G. (2009) X-ray crystallographic snapshots of reaction intermediates in pyruvate oxidase and transketolase illustrate common themes in thiamin catalysis. *J. Mol. Catal. B: Enzym. 61*, 93–99.
15. Kaplun, A., Binshtein, E., Vyazmensky, M., Steinmetz, A., Barak, Z., Chipman, D. M., Tittmann, K., and Shaanan, B. (2008) Glyoxylate carboligase lacks the canonical active site glutamate of thiamine-dependent enzymes. *Nat. Chem. Biol. 4*, 113–118.
16. Kluger, R., and Pike, D. C. (1977) Active-site generated analogues of reactive intermediates in enzymic reactions: Potent inhibition of pyruvate-dehydrogenase by a phosphonate analogue of pyruvate. *J. Am. Chem. Soc. 99*, 4504–4506.
17. Engel, S., Vyazmensky, M., Vinogradov, M., Berkovich, D., Bar-Ilan, A., Qimron, U., Rosiansky, Y., Barak, Z., and Chipman, D. M. (2004) Role of a conserved arginine in the mechanism of acetohydroxyacid synthase—Catalysis of condensation with a specific ketoacid substrate. *J. Biol. Chem. 279*, 24803–24812.
18. Bradford, M. M. (1976) Rapid and sensitive method for quantitation of microgram quantities of protein utilizing principle of protein-dye binding. *Anal. Biochem. 72*, 248–254.
19. Epelbaum, S., Chipman, D. M., and Barak, Z. (1990) Determination of products of acetohydroxy acid synthase by the colorimetric method, revisited. *Anal. Biochem. 191*, 96–99.
20. Bar-Ilan, A., Balan, V., Tittmann, K., Golbik, R., Vyazmensky, M., Hübner, G., Barak, Z., and Chipman, D. M. (2001) Binding and activation of thiamin diphosphate in acetohydroxyacid synthase. *Biochemistry 40*, 11946–11954.
21. Gollop, N., Barak, Z., and Chipman, D. M. (1988) Assay of products of acetolactate synthase. *Methods Enzymol. 166*, 234–240.
22. Barak, Z., Chipman, D. M., and Gollop, N. (1987) Physiological implications of the specificity of acetohydroxy acid synthase isozymes of enteric bacteria. *J. Bacteriol. 169*, 3750–3756.
23. Gollop, N., Damri, B., Barak, Z., and Chipman, D. M. (1989) Kinetics and mechanism of acetohydroxy acid synthase isozyme III from *Escherichia coli*. *Biochemistry 28*, 6310–6317.
24. Nemeria, N., Baykal, A., Joseph, E., Zhang, S., Yan, Y., Furey, W., and Jordan, F. (2004) Tetrahedral intermediates in thiamin diphosphate-dependent decarboxylations exist as a 1′,4′-imino tautomeric form of the coenzyme, unlike the Michaelis complex or the free coenzyme. *Biochemistry 43*, 6565–6575.
25. Nemeria, N. S., Chakraborty, S., Balakrishnan, A., and Jordan, F. (2009) Reaction mechanisms of thiamin diphosphate enzymes: Defining states of ionization and tautomerization of the cofactor at individual steps. *FEBS J. 276*, 2432–2446.
26. Tittmann, K., Golbik, R., Uhlemann, K., Khailova, L., Schneider, G., Patel, M., Jordan, F., Chipman, D. M., Duggleby, R. G., and Hübner, G. (2003) NMR analysis of covalent intermediates in thiamin diphosphate enzymes. *Biochemistry 42*, 7885–7891.
27. Arjunan, P., Sax, M., Brunskill, A., Chandrasekhar, K., Nemeria, N., Zhang, S., Jordan, F., and Furey, W. (2006) A thiamin-bound, pre-decarboxylation reaction intermediate analogue in the pyruvate dehydrogenase E1 subunit induces large scale disorder-to-order transformations in the enzyme and reveals novel structural features in the covalently bound adduct. *J. Biol. Chem. 281*, 15296–15303.
28. Kluger, R., and Tittmann, K. (2008) Thiamin diphosphate catalysis: Enzymic and nonenzymic covalent intermediates. *Chem. Rev. 108*, 1797–1833.
29. Frank, R. A. W., Titman, C. M., Pratap, J. V., Luisi, B. F., and Perham, R. N. (2004) A molecular switch and proton wire synchronize the active sites in thiamine enzymes. *Science 306*, 872–876.
30. Seifert, F., Golbik, R., Brauer, J., Lilie, H., Schröder-Tittmann, K., Hinze, E., Korotchkina, L. G., Patel, M. S., and Tittmann, K. (2006) Direct kinetic evidence for half-of-the-sites reactivity in the E1 component of the human pyruvate dehydrogenase multienzyme complex through alternating sites cofactor activation. *Biochemistry 45*, 12775–12785.
31. Jordan, F., Nemeria, N. S., and Sergienko, E. (2005) Multiple modes of active center communication in thiamin diphosphate-dependent enzymes. *Acc. Chem. Res. 38*, 755–763.
32. Muller, Y. A., Lindqvist, Y., Furey, W., Schulz, G. E., Jordan, F., and Schneider, G. (1993) A thiamin diphosphate binding fold revealed by comparison of the crystal-structures of transketolase, pyruvate oxidase and pyruvate decarboxylase. *Structure 1*, 95–103.
33. Muller, Y. A., and Schulz, G. E. (1993) Structure of the thiamine-dependent and flavin-dependent enzyme pyruvate oxidase. *Science 259*, 965–967.
34. Neumann, P., Weidner, A., Pech, A., Stubbs, M. T., and Tittmann, K. (2008) Structural basis for membrane binding and catalytic activation of the peripheral membrane enzyme pyruvate oxidase from *Escherichia coli*. *Proc. Natl. Acad. Sci. U.S.A. 105*, 17390–17395.
35. Xiang, S., Usunow, G., Lange, G., Busch, M., and Tong, L. (2007) Crystal structure of 1-deoxy-D-xylulose 5-phosphate synthase, a crucial enzyme for isoprenoids biosynthesis. *J. Biol. Chem. 282*, 2676–2682.
36. Arjunan, P., Nemeria, N., Brunskill, A., Chandrasekhar, K., Sax, M., Yan, Y., Jordan, F., Guest, J. R., and Furey, W. (2002) Structure of the pyruvate dehydrogenase multienzyme complex E1 component from *Escherichia coli* at 1.85 Angstrom resolution. *Biochemistry 41*, 5213–5221.
37. Arjunan, P., Umland, T., Dyda, F., Swaminathan, S., Furey, W., Sax, M., Farrenkopf, B., Gao, Y., Zhang, D., and Jordan, F. (1996) Crystal structure of the thiamin diphosphate-dependent enzyme pyruvate decarboxylase from the yeast *Saccharomyces cerevisiae* at 2.3 angstrom resolution. *J. Mol. Biol. 256*, 590–600.
38. Dobritzsch, D., König, S., Schneider, G., and Lu, G. G. (1998) High resolution crystal structure of pyruvate decarboxylase from *Zymomonas mobilis*—Implications for substrate activation in pyruvate decarboxylases. *J. Biol. Chem. 273*, 20196–20204.
39. Chabriere, E., Charon, M. H., Volbeda, A., Pieulle, L., Hatchikian, E. C., and Fontecilla-Camps, J. C. (1999) Crystal structures of the key anaerobic enzyme pyruvate:ferredoxin oxidoreductase, free and in complex with pyruvate. *Nat. Struct. Biol. 6*, 182–190.
40. Brandt, G. S., Nemeria, N., Chakraborty, S., McLeish, M. J., Yep, A., Kenyon, G. L., Petsko, G. A., Jordan, F., and Ringe, D. (2008) Probing the active center of benzaldehyde lyase with substitutions and the pseudosubstrate analogue benzoylphosphonic acid methyl ester. *Biochemistry 47*, 7734–7743.

41. Bruning, M., Berheide, M., Meyer, D., Golbik, R., Bartunik, H., Liese, A., and Tittmann, K. (2009) Structural and kinetic studies on native intermediates and an intermediate analogue in benzoylformate decarboxylase reveal a least motion mechanism with an unprecedented short-lived predecarboxylation intermediate. *Biochemistry 48*, 3258–3268.
42. Brandt, G. S., Kneen, M. M., Chakraborty, S., Baykal, A. T., Nemeria, N., Yep, A., Ruby, D. I., Petsko, G. A., Kenyon, G. L., McLeish, M. J., Jordan, F., and Ringe, D. (2009) Snapshot of a reaction intermediate: Analysis of benzoylformate decarboxylase in complex with a benzoylphosphonate inhibitor. *Biochemistry 48*, 3247–3257.
43. Fiedler, E., Thorell, S., Sandalova, T., Golbik, R., König, S., and Schneider, G. (2002) Snapshot of a key intermediate in enzymatic thiamin catalysis: Crystal structure of the alpha-carbanion of (alpha, beta-dihydroxyethyl)-thiamin diphosphate in the active site of transketolase from *Saccharomyces cerevisiae*. *Proc. Natl. Acad. Sci. U.S.A. 99*, 591–595.
44. Asztalos, P., Parthier, C., Golbik, R., Kleinschmidt, M., Hübner, G., Weiss, M. S., Friedemann, R., Wille, G., and Tittmann, K. (2007) Strain and near attack conformers in enzymic thiamin catalysis: X-ray crystallographic snapshots of bacterial transketolase in covalent complex with donor ketoses xylulose 5-phosphate and fructose 6-phosphate, and in noncovalent complex with acceptor aldose ribose 5-phosphate. *Biochemistry 46*, 12037–12052.
45. Frank, R. A. W., Leeper, F. J., and Luisi, B. F. (2007) Structure, mechanism and catalytic duality of thiamine-dependent enzymes. *Cell. Mol. Life Sci. 64*, 892–905.